Secondary Gas Injection Effect on Dual-Bell Nozzle Flow Transition

Emanuele Martelli⋆*, Francesca Scaramuzzino*⋆ *and Francesco Nasuti*⋆⋆
⋆ *Second University of Naples*
Department of Aerospace and Mechanical Engineering, Via Roma 29, 81131, Aversa, Italy
⋆⋆ *University of Rome "La Sapienza"*
Department of Mechanical and Aerospace Engineering, Via Eudossiana 18, 00184, Rome, Italy

Abstract

Dual bell nozzles represent a possible solution to improve the performance of large liquid rocket engines for launcher first stages. During the low-altitude mode, the flow is separated and the separation line is located near the inflection of the nozzle wall, in a region characterized by a negative value of the wall pressure gradient and where side loads may occur. At high altitude the flow attaches to the nozzle wall and the full area ratio is used. The flow behavior during the transition between the two operating modes is analyzed by time-accurate simulations carried out on an axi-symmetric geometry and considering two configurations: one with a wall film cooling and the other without film. Aim of this study is to analyze the effect of the secondary gas injection on the dynamics of the separation point and on the transition time. Results show that film injection may substantially change the characteristic transition time and evolution.

1. Introduction

A well proven way of slightly improving performance of gas-generator open-cycle engines is the injection of the turbine exhaust gas (TEG) into the main nozzle. The role of TEG is twofold: besides to the performance increase, it provides a low temperature gas able to create an insulating film that reduces the convective heat transfer rate from the hot gas stream to the exposed nozzle surface [1]. The basic studies on TEG injection have addressed cooling properties and nozzle performance during design operations in conventional nozzles. However, following the development in advanced nozzle studies [2, 3], a renewed investigation is required to understand the role of film injection in nozzles operating in overexpanded conditions with flow separation. This is the case for dual bell nozzles, for which a detailed parametric analysis of the film cooling in both sub- and full-scale hot dual bell nozzles has been carried out [4, 5]. The dual bell nozzle divergent section features two bells with different exit area, whose geometries are connected by an inflection point. In this way two different operating modes can be achieved: at low altitude the flow is attached in the first bell and separated downstream the inflection point, while at high altitude the nozzle operates with attached flow in the whole divergent section.

The main results of the "high-altitude" operation studied [4, 5] are that film cooling is efficient, also thanks to the centered expansion at the inflection point. Moreover, the analysis of design operation indicates that film cooling has an effect on the overexpanded operation of the nozzle. In particular, it could enhance the onset of side loads when the dual bell operates in the first mode with the separation point anchored at the wall inflection. In fact, the real behavior of the wall pressure is different from the theoretical one: due to viscosity, the ideal wall pressure step at the inflection point becomes a region of finite length, where the pressure gradient is negative as in conventional nozzles. In this region, which has been referred to as inflection region [6], the separation point finds stable but not symmetric equilibrium positions because of the inevitable flow asymmetries, and thus side loads can occur like in the case of conventional bell nozzles. The qualitative behavior of these side loads has been numerically predicted [5, 7] and then experimentally confirmed in [8]. It has also been shown that the separation point could spend a long period in the inflection region (of the order of 10 seconds) due to the fact that its movement is governed by the ambient pressure variation during the flight trajectory [9]. During this period the nozzle can experience long lasting side loads, unless thrust throttling is considered.

Numerical and experimental studies [6, 10] focused their attention on the time duration of the transition between the two operating modes. In particular, they divided the transition time in the time the separation point spends in moving from the inflection point up to the end of the inflection region (also defined as sneak transition in [10]) and the time it spends in moving to the final equilibrium location at the nozzle lip. The former time takes into account the evolution of the separation point in the inflection region, that is the region where it can assume stable locations, depending on the chamber to ambient pressure ratio, defined as nozzle pressure ratio *PR*. A recent study has shown that the film cooling pressure can shifts the mode transition to higher values of the nozzle pressure ratio [11].

In the present investigation, starting from steady-state simulations, time accurate Reynolds Average Navier-Stokes (RANS) simulations of the transition of the separation point are carried out considering dual bell nozzle configurations with and without film cooling. Aim of this analysis is to understand the influence of the injection of the secondary gas on the dynamics of the separation point. In particular the variation of the transition nozzle pressure ratio and the transition time induced by different film Mach numbers is computed and assessed.

2. Numerical method

The analysis of dual bell nozzle flowfield is performed by an in-house 2-D time-accurate Reynolds Averaged Navier-Stokes solver, based on the approach described in Ref. [12, 13, 14] and validated for the study of overexpanded flows [15]. The main features of this method are to discretize the convective terms according to the lambda scheme developed by Moretti [16]. This numerical scheme is second order accurate both in space and in time. The discontinuities are solved via a finite volume Godunov method (hybrid formulation [12, 17]). The viscosity is described by the Sutherland's law. Turbulence is computed by the Spalart-Allmaras one-equation model [18].

3. Test case description

This study is carried out considering a 2D axisymmetric cold gas sub-scale nozzle, whose geometric properties and operating conditions are reported in Table 1. The main data (base and extension lengths and the inflection angle) are taken from the experimental study described in [10]. The base nozzle has been designed as a truncated ideal contour nozzle, while the extension has been designed with an assigned constant wall pressure gradient. This kind of geometry will be referred to as Linearly Increasing wall Pressure (LIP) dual bell nozzle. Both the base and the extension have been designed with the method of characteristics [6].

Table 1: Geometric and Operating conditions of the LIP dual bell nozzle

Throat radius r_t	0.01 m
Nondimensional base length l_b/r_t	5.2
Base area ratio ε_b	9.6
Nondimensional extension length l_e/r_t	8.3
Inflection angle α	9 deg
Nondimensional extension wall pressure gradient	$1.6 \cdot 10^{-4}$
Extension area ratio ε_e	23.1
Nondimensional total length l_t/r_t	13.5
Feeding gas	Nitrogen
Feeding pressure p_0	2.3-3.2 MPa
Feeding temperature T_0	300 K
Ambient pressure p_a	0.1 MPa

In the film cooled dual bell nozzle, the injection is made through an axisymmetric slot with height equal to 0.94 mm, located in the base at a nondimensional distance from the throat $x_{film}/r_t = 3.5$ (in the following all the abscissas will be taken from the throat), where the expansion area ratio is $\varepsilon_{x_{film}} = 6$. The injection is made at a supersonic velocity and with a value of the static pressure such that the secondary injection is adapted with the main flow. In Table 2 the film Mach numbers (M_f) are reported together with the nondimensional inlet static pressure (p_f/p_0), non dimensional temperature (T_f/T_0) and the ratio between the film and main mass flow ($\dot{m}_f/\dot{m}_m$). The film mass flow can be expressed

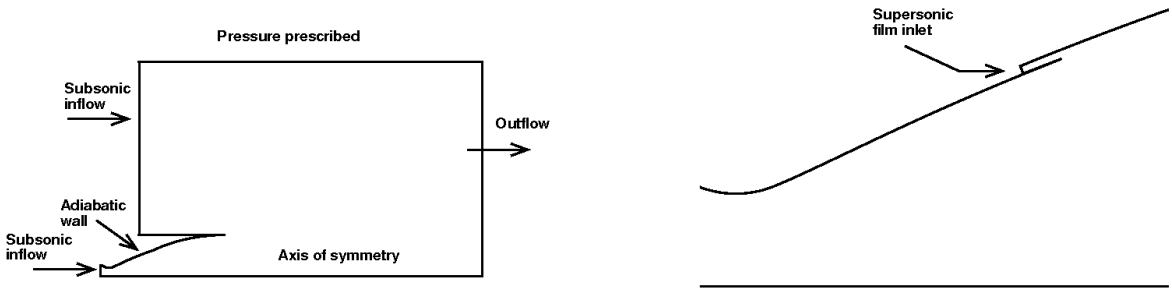

Figure 1: Geometry and boundary conditions, left: clean configuration, right: film cooled configuration.

as a function of p_f, T_f and M_f by the isentropic relations:

$$\dot{m}_f = \left(\frac{\gamma}{RT_f}\right)^{\frac{1}{2}} p_f A_f M_f \tag{1}$$

where γ is the ratio of the specific heats, R is the gas constant and A_f is the film inlet area. The film total temperature

Table 2: Film Mach number, inlet static pressure, temperature and mass flow ratio.

M_f	p_f/p_0	T_f/T_0	$\dot{m}_f/\dot{m}_m$ (%)
1.1	0.0308	0.346	4.0
1.4	0.0308	0.308	5.5
1.7	0.0308	0.272	7.7

is kept constant when the film Mach number is changed, therefore the film static temperature decreases when M_f increases. On the contrary, as the secondary jet is assumed to remain adapted, the static pressure is kept constant and the film total pressure increases with the film Mach number. Figure 1(a) shows the selected geometry, the computational domain and the assigned boundary conditions for the case with and without film cooling. The latter will be addressed to as clean configuration. Figure 1(b) shows an enlargement of the arrangement for the film slot. The external domain is characterized by a subsonic inflow boundary condition (total temperature and total pressure are enforced together with the flow direction) on the left side, assigned pressure on the top boundary (whose height is four times the nozzle lip radius), and non-reflecting boundary conditions on the right side (whose distance from the nozzle exit is equal to six times the nozzle lip radius). The nozzle is characterized by a subsonic inflow boundary condition, an axis of symmetry and an adiabatic wall. A supersonic inflow condition is enforced at the film injection inlet: the film Mach number, the static pressure, the static temperature and the flow direction are imposed. To simulate the slot for the secondary gas injection, Figure 1(b), the wall profile is translated outward from the injection point to the nozzle end. Before mixing a zero-thickness adiabatic wall, 4.1 mm long, divides the main and film flows.

4. Discussion of the results

4.1 Flowfield description

Figure 2 shows the Mach number flowfields for the clean case at two different feeding to ambient pressure ratios (PR= p_0/p_a). At PR= 23 (left) the separation point is anchored at the inflection and the divergent section is filled with the

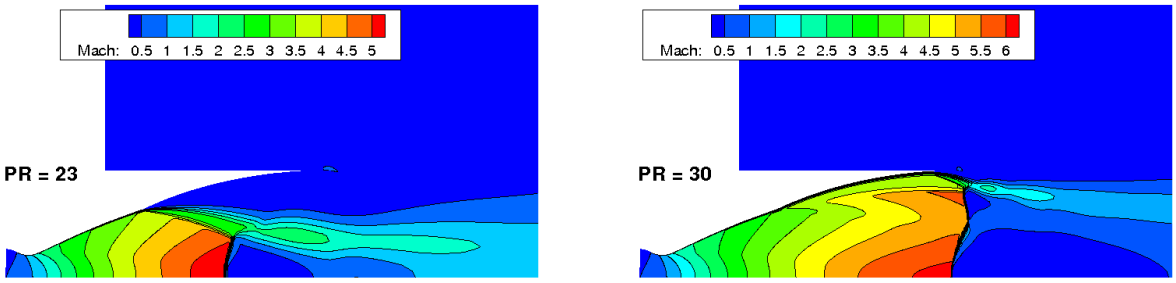

Figure 2: Clean configuration. (Left): Mach number flowfield at PR= 23: separation point anchored at the inflection; (Right): Mach number flowfield at PR= 30: separation point at the nozzle lip.

back flow from the ambient. At PR= 30 the flow is attached to the nozzle extension wall and the separation point is located at the nozzle lip. Figure 3 shows the Mach number flowfield in a film cooled case with M_f= 1.7 and PR = 28. The shear layer between the main and the secondary stream, which then interacts with the flow separation at the inflection point, can be easily seen in the figure. The fully attached steady-state wall pressure profiles, together with their gradients, for the clean and the film-cooled configurations are plotted in Figure 4 (left). It appears that the inflection region length increases with the secondary injection. This increase is quantified in Table 3: in the film-cooled case l_i increases from 24% to 27% with respect to the clean case. It can also be seen from the table that l_i is only slightly affected by the film Mach number value. It is interesting to note that the increase in the film Mach number changes the shape of the inflection region, as shown better in Figure 4 (right). This picture reports the wall pressure gradient of the clean configuration and of the case with M_f= 1.7, which is the one with the largest modification. It is evident that the effect of the secondary gas injection is to reduce the modulus of the pressure gradient in the first part of the inflection region with respect to the clean case. This has a direct effect on the dynamics of the separation point, as will be discussed in the following.

Table 3: Inflection region length.

	l_i/r_t	$l_{i,film}/l_{i,clean}$
Clean	1.35	1.
M_f = 1.1	1.68	1.24
M_f = 1.4	1.72	1.27
M_f = 1.7	1.68	1.24

4.2 Transition by a sequence of steady-state computations

The sequence of steady-state solutions is obtained by increasing the feeding total pressure and keeping constant the ambient pressure. In the case with film cooling, the film static pressure is always set equal to the main flow static pressure. Therefore the secondary and the main mass flow rates increase proportionally and their ratio remains constant. Table 4 reports the film static pressures and the film mass flow rate for the different pressure ratios for each film Mach number. The results of the simulation are reported in Figure 5 (left), which shows the separation point abscissa (x_{sep}) as a function of PR. As can be seen from the picture, the separation point finds stable solutions in the inflection region, whose length is equal to 1.35 cm without film cooling and approximately to 1.7 cm with film cooling. Then, when the separation point enters in the positive pressure gradient region, it jumps toward the second bell exit. Figure 5 (right) shows the transition pressure ratio (PR_{trans}) as a function of M_f: in the clean case PR_{trans} is equal to 28, while in the film-cooled configurations the PR_{trans} increases up to 31 for M_f= 1.1, to 32 for M_f= 1.4 and then again 31 for M_f= 1.7. Therefore, the global effect of the secondary gas injection is to increase the transition pressure ratio, as also stated by [11].

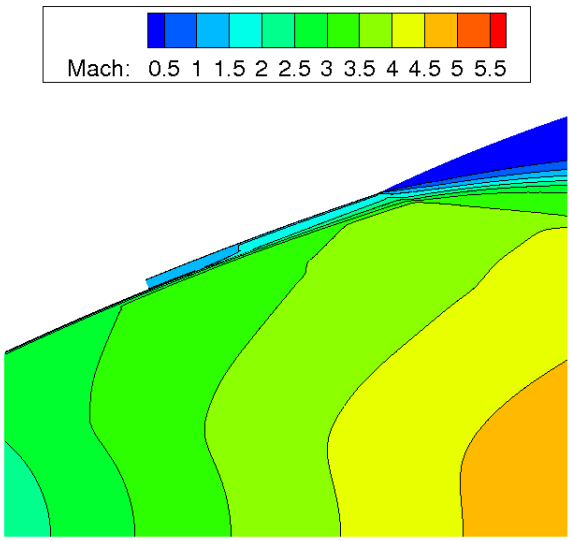

Figure 3: Mach number flowfield of the film cooled configuration (M_f=1.7) at PR = 28.

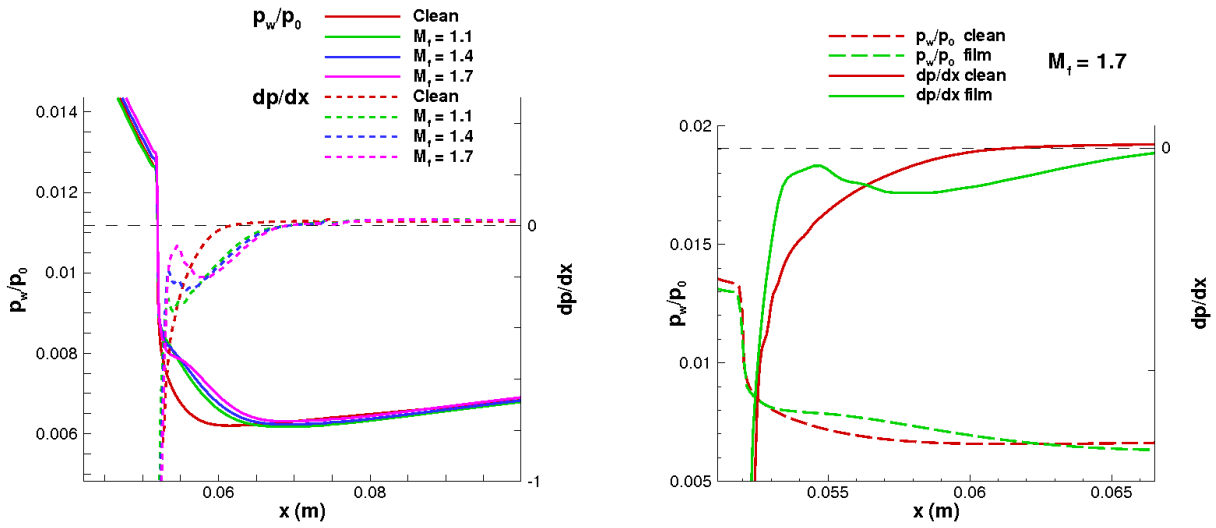

Figure 4: (Left): Wall pressure profiles and their gradients with and without film cooling for the fully attached mode; (Right): Enlargement of the wall pressure and pressure gradient profiles for the clean case and for the case with M_f=1.7.

Table 4: Film Mach number, inlet static pressure, and mass flow rate.

M_f	PR	p_f (MPa)	$\dot{m}_f$ (kg/s)
1.1	28	0.086	0.082
1.1	29	0.089	0.085
1.1	30	0.092	0.088
1.1	31	0.095	0.091
1.4	28	0.086	0.110
1.4	29	0.089	0.114
1.4	30	0.092	0.118
1.4	31	0.095	0.122
1.4	32	0.099	0.126
1.7	28	0.086	0.143
1.7	29	0.089	0.148
1.7	30	0.092	0.153
1.7	31	0.095	0.158

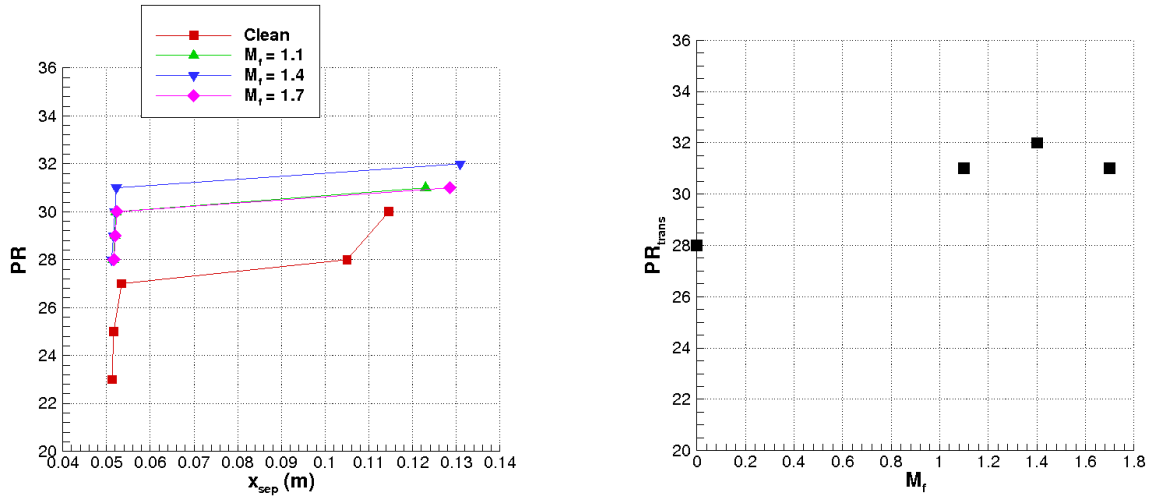

Figure 5: (Left): Separation point abscissas as a function of the pressure ratio PR for the clean and the film-cooled cases; (Right): Transition pressure ratio as a function of M_f.

4.3 Transition by time-accurate computations

In the present time-accurate simulations the nozzle pressure ratio is again varied by increasing the feeding total pressure while keeping constant the ambient pressure. The transition has been computed for the clean case and for the film-cooled case with M_f= 1.7. The starting point is PR = 26.4 for the clean case and PR = 30 for the case with film cooling. These pressure ratios have been chosen such that the separation point is located in the inflection region, where the pressure gradient is approximately equal in modulus to 10% of the maximum gradient value (which is located at the inflection point). The resulting nondimensional abscissa x_{init}/r_t is equal to 5.26 and $(x_{init} - x_{inflection})/r_t$ = 0.06 and is the same for both cases. This location is rather arbitrary, it only serves to indicate where the inflection region is characterized by a negative pressure gradient with the same order of magnitude that can be found in conventional nozzles. The final pressure ratio is the transition pressure ratio: PR = 28 for the clean case and 31 for the film-cooled case. The total pressure is linearly increased in 0.5 ms for both cases. In such a way the $\Delta PR/\Delta t$ is equal to 3.2 $(\text{ms})^{-1}$ for the clean case and 2 $(\text{ms})^{-1}$ for the film-cooled case. The exact value of these gradients, as demonstrated by foregoing studies, is not important for the present analysis. In fact, they have the meaning of the numerical implementation of a sudden jump of the pressure ratio (like a step function). The Mach number flowfield evolution with time for the configuration with M_f= 1.7 is shown in Figure 6, where the plots are relevant to times separated each other by a constant time interval of 1 ms, while Figure 7 shows the separation point abscissas and velocities as a function of the elapsed time for both configurations. The sudden pressure ramping is fast enough (3.2 bar/ms and 2 bar/ms for the case without and with film, respectively), such that when the final pressure is reached (t = 0.5 ms), the separation point is still in the inflection region, as can be seen from Figures 6 and 7. After leaving the inflection region, the separation point enters the region with linearly increasing wall pressure, reaching its maximum velocity. Finally, the separation point decelerates approaching the nozzle lip.

The total transition time $t_{tr,\ tot}$ is defined as the time elapsed from the instant when the separation point leaves its initial location up to the instant when it reaches its maximum abscissa near the exit of the second bell. As already done in [6], the transition time is split in the time $t_{tr,1}$ the separation point spends in the inflection region and the time $t_{tr,2}$ the separation point spends in the nozzle extension. Table 5 reports the transition times, together with the maximum velocity and the velocity averaged over the total transition time. In the clean configuration the total transition lasts

Table 5: Transition times and velocity of the separation point

	$t_{tr,1}$ (ms)	$t_{tr,2}$ (ms)	$t_{tr,tot}$ (ms)	v_{max} (m/s)	v_{av} (m/s)
Clean	3.8	10.7	14.5	5.2	3.8
Film cooled	1.4	1.3	2.7	61.7	28.5

14.5 ms (3.8 ms are spent in the inflection region) with a maximum velocity of 5.2 m/s and an average velocity of 3.8 m/s. These values are of the same order of magnitude of the experimental data reported in [19], where an extension of similar length is adopted. In the film-cooled configuration the dynamics of the separation point is similar, but the velocity of the separation front is much higher than that of the clean configuration. The maximum velocity (61.7 m/s) is approximately one order of magnitude higher than the value of the clean configuration, and the same is true for the average velocity (28.5 m/s). The times $t_{tr,1}$ and $t_{tr,2}$ are equal to 1.4 ms and 1.3 ms respectively, showing that in the film cooled configuration the transition in the positive pressure gradient region is very fast. Therefore the secondary gas injection at a high Mach number (M_f= 1.7) decreases the time spent by the separation point both in the inflection region and in the region with positive pressure gradient, with respect to the clean case. The larger acceleration that the separation point experiences in the inflection region of the film-cooled case is caused by the wall pressure gradient modified by the secondary gas injection, as shown in Figure 4 (right): in the first part of the inflection region, from x/r_t= 5.27 to x/r_t= 5.63 (approximately the first 20% of $l_{i,\ film}$), this gradient is lower in modulus and closer to the zero value than in the clean case. The increase in the chamber pressure forces the separation point to move downstream towards a new equilibrium position and the lower the pressure gradient modulus, the larger the region where the separation point is in non-equilibrium. As a consequence, in the film-cooled case the separation front reaches a higher velocity than in the clean case. It must be noted that this conclusion holds in the case where the pressure ramping is very fast and such that the separation point can not find stable equilibrium position inside the inflection region. On the contrary, as stated above, in a real application the movement of the separation front is governed by the ambient pressure variation, which is very slow and the separation point dynamics can be approximated as a sequence of steady state positions. In such a situation, the larger inflection region and the wall pressure gradient of the film-cooled configuration increase the side

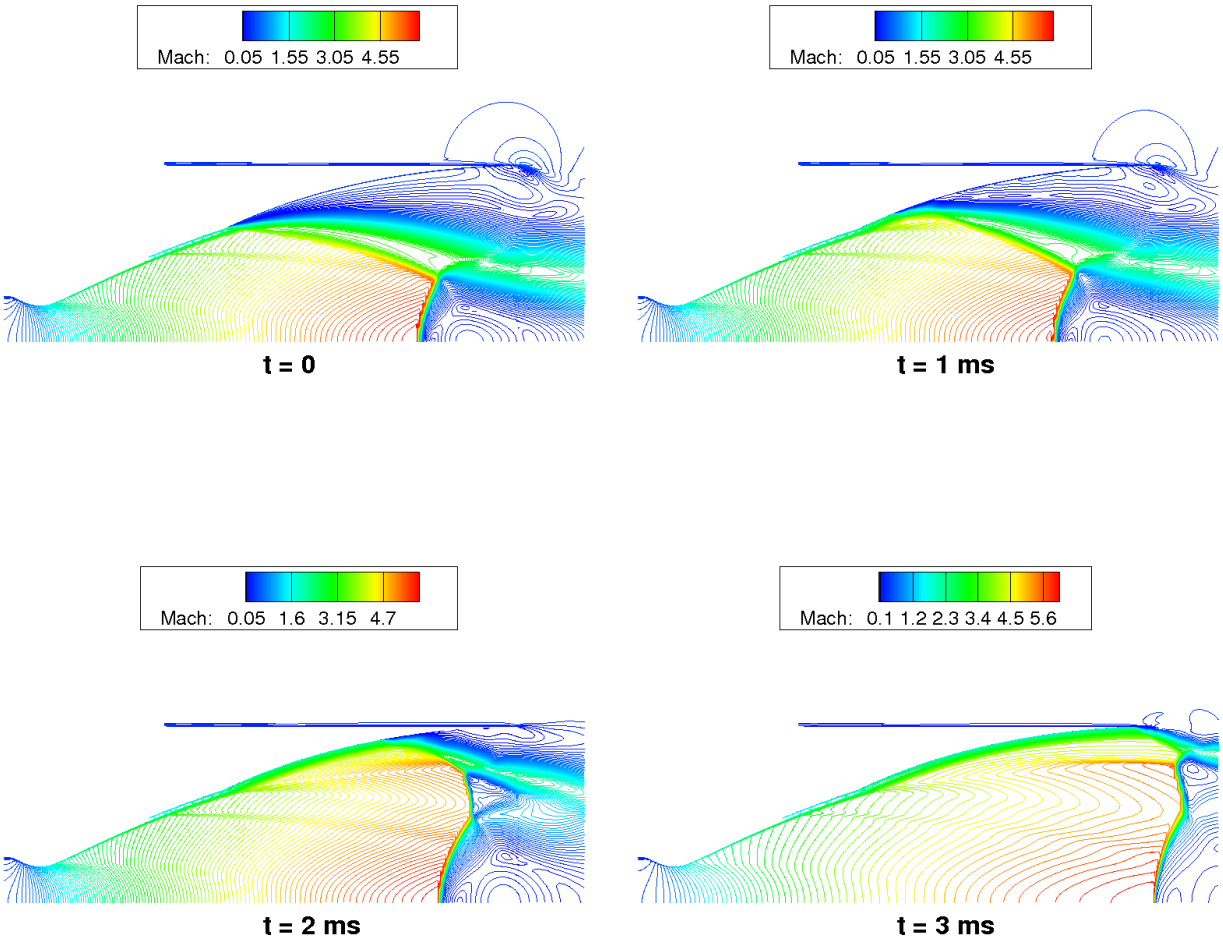

Figure 6: Mach number flowfield evolution with time of the film-cooled configuration with M_f= 1.7.

load intensity [5]. In the non equilibrium case (very fast pressure ramping), the wall pressure gradient modified by the secondary gas injection increases the side loads but makes them to be applied for a shorter time.

5. Conclusions

The transition between the two operating modes of a dual bell nozzle, for both a film-cooled and a clean configuration, has been computed considering a cold gas sub-scale configuration and both steady state and time accurate simulations. The steady state results show that the injection of a secondary gas shifts the transition pressure ratio toward higher values. On the contrary, changing the film Mach number slightly affects the transition pressure ratio (like an on-off effect). The time accurate simulations considered the clean case and the film-cooled configuration with M_f= 1.7. The results lead to the following conclusions: the injection of the secondary gas upstream of the wall inflection point at high Mach number makes the inflection region wider but increases the velocity of the separation point, which moves because of an abrupt chamber pressure increase. In fact, the transition time is reduced by a factor of 5 with respect to the case without injection. This reduction is due to the wall pressure gradient in the inflection region, which is closer to zero than in the clean case, and then it allows the separation point to reach a higher velocity. In such a configuration therefore, the film cooling does help to make the transition faster. This is true only when the pressure ramping is very

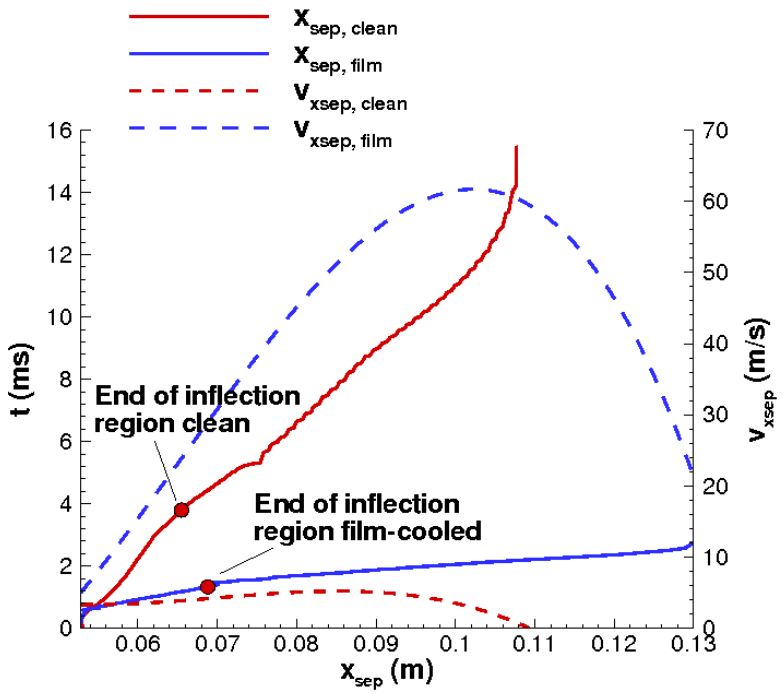

Figure 7: Time history of the separation point abscissas and velocities for the clean and film-cooled configurations.

fast, such that the separation point can never find equilibrium position in the inflection region.

References

[1] O'Connor, J. P. and Haji-Sheikh, A., "Numerical Study of Film Cooling in Supersonic Flow," *AIAA Journal*, Vol. 30, No. 10, 1992.

[2] Muss, J. A., Nguyen, T. V., Reske, E. J., and McDaniels, D. M., "Evaluation of Altitude Compensating Nozzle Concepts for RLV," AIAA Paper 97–3222, Jul. 1997, 33rd AIAA/ASME/SAE/ASEE Joint Propulsion Conference & Exhibit.

[3] Hagemann, G., Immich, H., Nguyen, T. V., and Dumnov, G. E., "Advanced Rocket Nozzles," *Journal of Propulsion and Power*, Vol. 14, No. 5, Sep-Oct 1998, pp. 620–634.

[4] Nasuti, F., Martelli, E., Onofri, M., and Pietropaoli, E., "Film Cooling in Dual Bell Nozzle," *Proc. 5th European Symp. on Aerothermodynamics for Space Vehicles, November 2004*, ESTEC, ESA SP-563, Noordwijk, The Netherlands, 2005.

[5] Martelli, E., Nasuti, F., and Onofri, M., "Numerical Analysis of Film Cooling in Advanced Rocket Nozzles," *AIAA Journal*, Vol. 47, No. 11, 2009, pp. 2558–2604.

[6] Nasuti, F., Onofri, M., and Martelli, E., "Role of Wall Shape on the Transition in Axisymmetric Dual-Bell Nozzles," *Journal of Propulsion and Power*, Vol. 21, No. 2, 2005, pp. 243–250.

[7] Martelli, E., Nasuti, F., and Onofri, M., "Numerical Parametric Analysis of Dual-Bell Nozzle Flows," *AIAA Journal*, Vol. 45, No. 3, 2007, pp. 640–650.

[8] Stark, R. and Nürnberger-Genin, C., "Side Loads in Dual Bell Nozzles, Part I: Phenomenology," AIAA Paper 2010-6729, Jul. 2010, 46th AIAA/ASME/SAE/ASEE Joint Propulsion Conference.

[9] Martelli, E., Nasuti, F., and Onofri, M., "Thermo-Fluid-Dynamics Analysis of Film Cooling in Overexpanded Rocket Nozzles," AIAA Paper AIAA-2006-5207, Jul. 2006, 42th AIAA/ASME/SAE/ASEE Joint Propulsion Conference and Exhibit.

[10] Nürnberger-Genin, C. and Stark, R., "Flow Transition in Dual Bell Nozzle," *Shock Waves*, Vol. 19, No. 3, 2008, pp. 265–270.

[11] Proshchanka, D., Yonezawa, K., Koga, H., Tsukuda, H., Tsujimoto, Y., Kimura, T., Yokota, K., and Pasini, A., "Control of Operation Mode Transition in Dual-Bell Nozzle with Film Cooling," AIAA Paper 10–6815, Jul. 2010, 46th AIAA/ASME/SAE/ASEE Joint Propulsion Conference.

[12] Martelli, E., *Studio della Fluidodinamica Interna di Ugelli Propulsivi di Tipo Dual Bell*, January 2006, PhD Dissertation, Università degli studi di Roma *"La Sapienza"*.

[13] Nasuti, F. and Onofri, M., "Analysis of Unsteady Supersonic Viscous Flows by a Shock Fitting Technique," *AIAA Journal*, Vol. 34, No. 7, Jul. 1996, pp. 1428–1434, See also AIAA Paper 95–2159.

[14] Nasuti, F., "A Multi-Block Shock-Fitting Technique to Solve Steady and Unsteady Compressible Flows," *Computational Fluid Dynamics 2002*, edited by S. Armfield, P. Morgan, and K. Srinivas, Springer-Verlag, Berlin, 2003, pp. **217–222**.

[15] Martelli, E., Nasuti, F., and Onofri, M., "Numerical Calculation of FSS/RSS Transition in Highly Overexpanded Rocket Nozzle Flows," *Shock Waves*, Vol. 20, No. 2, 2010, pp. 139–146.

[16] Moretti, G., "A Technique for Integrating Two-Dimensional Euler Equations," *Computer and Fluids*, Vol. 15, No. 1, 1987, pp. 59–75.

[17] Paciorri, R., *Sviluppo di una metodologia numerica in forma quasi-lineare e analisi di modelli termochimici per lo studio di flussi viscosi ipersonici*, Febbraio 1995, Tesi di Dottorato, Università degli studi di Roma *La Sapienza*.

[18] Spalart, P. R. and Allmaras, S. R., "A One-Equation Turbulence Model for Aerodynamic Flows," *La Recherche Aerospatiale*, , No. 1, 1994, pp. 5–21.

[19] Nürnberger-Génin, C. and Stark, R., "Experimental study on dual bell nozzle," *Proceedings of the 2nd European Conference for Aero-space Science, Brussels, Belgium, 1st-6th July 2007*.